SUPPORTING INFORMATION

Enhanced Performance of Si MIS Photocathodes Containing Oxide-Coated Nanoparticle Electrocatalysts

Natalie Y. Labrador,[1] Xinxin Li,[1] Yukun Liu,[1] Haiyan Tan,[2] Rongyue Wang,[2] Jeffery T. Koberstein,[1] Thomas P. Moffat,[2] and Daniel V. Esposito[1]*

[1]Department of Chemical Engineering,
Lenfest Center for Sustainable Energy,
Columbia University in the City of New York
500 W. 120th St., New York, NY 10027
*de2300@columbia.edu

[2]Materials Measurement Laboratory,
National Institute of Standards and Technology
100 Bureau Drive, Gaithersburg, MD 20878

Table of Contents

I. SiO_x/Pt/native SiO_2/Si synthesis procedures

1.1 SiO_2/Si electrode preparation

Monocrystalline p-type Si(100) wafers (1-5 Ω cm, 500-550 µm thick, WRS materials) were cleaved into 1.5 × 2 cm pieces. A diamond scribe was used to scratch and remove native oxide on the back side. An electrical back contact was made with indium solder and a copper wire. Back contact resistance was typically ≈ 12 Ω. Finally, the wafers were sealed in 3M Electroplater's tape to protect the back contact and create a well-defined 0.246 cm^2 circular opening on the front of the electrode for PEC measurements.

1.2 Platinum (Pt) photoelectrodeposition

All electrochemical measurements were performed using a SP-200 BioLogic potentiostat controlled by EC-Lab v10.40 software. Photoelectrodeposition was carried out in a Pt plating solution, 3 mmol L^{-1} potassium tetracholoroplatinate (K_2PtCl_4, Sigma Aldrich, ACS reagent) with 0.5 mol L^{-1} sodium chloride (NaCl, Sigma Aldrich, ACS reagent) as supporting electrolyte and under approximately 1 sun intensity by a Xe arc lamp. The solution was modified with hydrochloric acid (HCl, Sigma Aldrich) to pH 3.5 and bubbled with nitrogen gas for 20 minutes to purge dissolved oxygen. A Pt mesh (Alfa Aesar, 99.9%) and glass frit-isolated Ag|AgCl/sat. 3 mol L^{-1} KCl were used as a counter and reference electrode respectively. AM 1.5G illumination was achieved with a 300 W xenon arc lamp (Newport, 67005) and AM 1.5G filter (Newport, 81094) in a Newport housing powered by a power supply (Newport, 69911). The intensity was calibrated to 100 mW cm^{-2} with solar reference cell (VLSI Standards, SRC-1000-RTD-QZ). Light was used to irradiate and assist electrodeposition on p-type Si.

Figure S1 shows cyclic voltammetry (CV) curves for SiO_2/p-Si (100) in 3 mmol L^{-1} potassium tetracholoroplatinate. Pt was electrodeposited by performing CV between -50 mV to -

450 mV vs. Ag|AgCl with a 50 mV s^{-1} scan rate. The number of CV cycles was varied, 5, 10, and 20 cycles, to produce the different platinum loadings, 1, 5, and 20 µg cm^{-2} (Fig. S1a-c). This deposition potential range was determined by two CV curves conducted in the deposition solution over a wider potential window, +450 mV to -800 mV, for a fresh sample (Fig. S1d). In the first scan, reduction current corresponding to the onset of Pt deposition is observed at ≈ -0.4 V vs. Ag|AgCl, and shifts to +0.4 V vs. Ag|AgCl in the second scan. This shift can be attributed to the difference in nucleation kinetics for Pt on the SiO_2 surface compared to deposition on Pt particles that were present during the second scan.

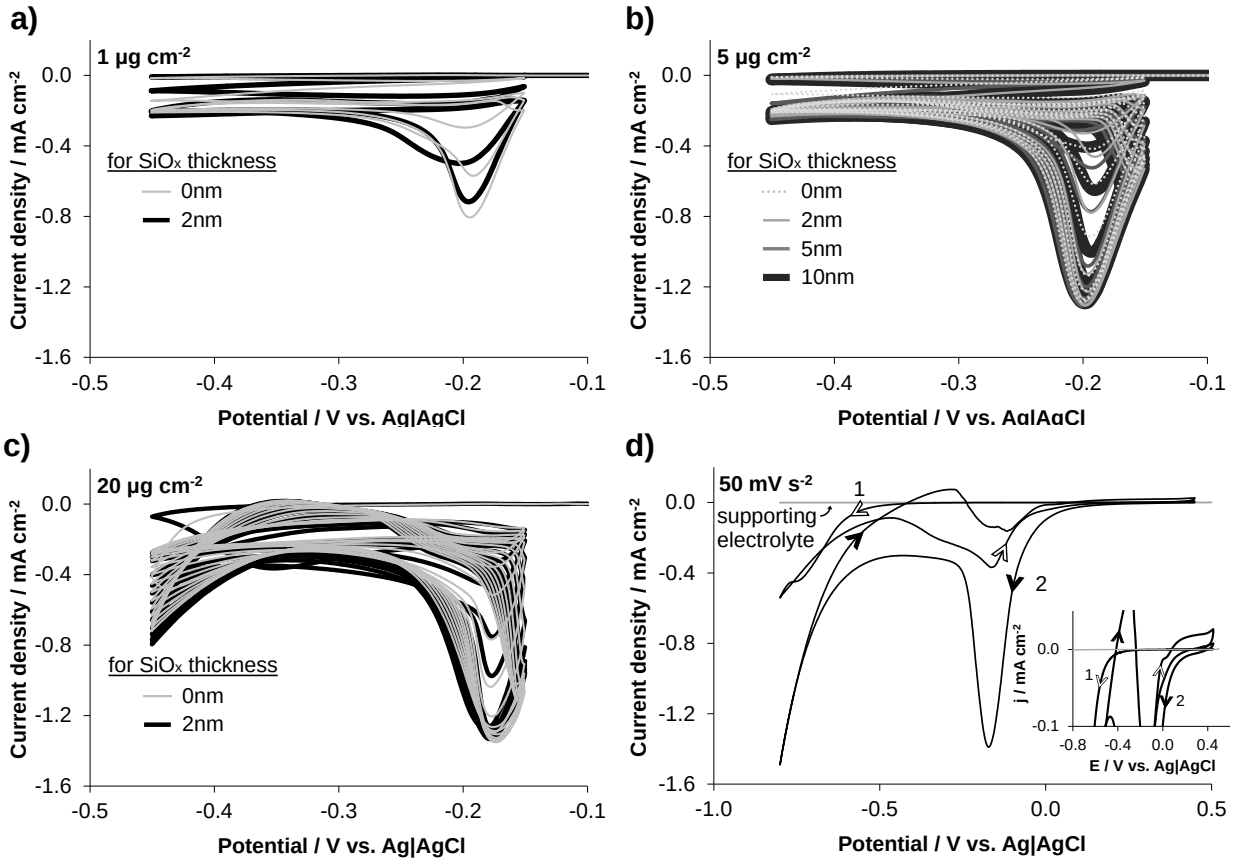

Figure S1. CV and LSV in electrodeposition solution. Current-potential curves for SiO_2/p-Si (100) in 3 mmol L^{-1} potassium tetracholoroplatinate. CV scan between -50 mV to -450 mV vs. Ag|AgCl at 50 mV s^{-1} scan rate for a) 5, b) 10, and c) 20 cycles. d) CV scan between +450 mV to -800 mV Ag|AgCl at 50 mV s^{-1} scan rate to determine potential range for electrodeposition. Inset zooms in on the onset potentials for Pt deposition in scans 1 and 2.

1.3 PDMS spin coating procedure

Trimethylsiloxy terminated polydimethylsiloxane (PDMS) was spin coated onto electrodeposited Pt/p-Si substrates at a speed of 2000 rpm for 1 min from a toluene solution.[1,2] The concentration of PMDS/toluene solution, 1.4 mg ml^{-1}, 2.8 mg ml^{-1}, 4.5 mg ml^{-1}, was selected to produce SiO_x films with thickness of 2 nm, 5 nm, and 10 nm respectively. The samples were then dried in a vacuum oven at 70 °C for 60 minutes to evaporate the solvent. Afterwards, the PDMS was converted to SiO_x in a ultraviolet/ozone (UV-ozone) cleansing chamber for 2 hours (UVOCS, T10X10/OES) which generates UV light in the 254 nm and 185 nm range.[1,3] The thickness of the SiO_x film was measured with an alpha-SE® Ellipsometer and fit with Cauchy model.

1.4 Electron beam (e-beam) evaporated metal layers

Continuous metallic films (for ferri/ferrocyanide measurements) and ordered arrays of circular metallic dots (for effective diffusion length measurements) were deposited onto native SiO_2/p-Si(100) wafers at 0.2 A s^{-1} by e-beam evaporation in a Angstrom EvoVac evaporator system with a base pressure of 1.0×10^{-7} torr. The patterned samples were made by evaporating the metal through single layer shadow masks possessing circular holes with 0.5 mm diameters. 3 nm thick Pt (99.99%) and 2 nm thick Ti (99.99%) layers were sequentially deposited without breaking vacuum and without substrate heating. Film thicknesses were monitored with quartz crystal thickness monitors.

II. Characterization of MIS and IMIS samples

2.1 Scanning electron microscopy (SEM)

SEM was carried out with a Hitachi S4700 field emission SEM microscope. Figure S2 contains SEM images performed on MIS structures with 1, 5, and 20 μg cm^{-2} of electrodeposited Pt. SEM images of several locations for every sample were analyzed with a MatLab image analysis

program to characterize Pt nanoparticle coverage, density (particles μm^{-2}), diameter, spacing, surface area (cm^2 Pt per geometric cm^2) and loading. The image analysis software approximates each particle as a circle, returning its effective diameter. Particle loading values were estimated based on the measured particle diameters, the density of Pt (21.45 g cm^{-3} Pt), a void fraction of 0.54,[4] and assuming a hemispherical particle geometry. The hemispherical geometry is a reasonable approximation based on typical particle shape observed in cross-sectional SEM and TEM. The reported average particle separation distances between neighboring particles were estimated as the distance between particles if all detected particles in an SEM image were positioned in a square lattice arrangement where all particles are equidistant. The particle coverage, density, distance, surface area, and loading are reported as averages over 8 different areas (SEM images) on each sample and the standard deviation between these different areas. The particle density, Pt particle surface area, and loading are normalized with respect to electrode geometric area of the exposed electrode. The reported particle diameters were calculated as an averages of all the effective particle diameters of >1000 particles from 8 different areas.

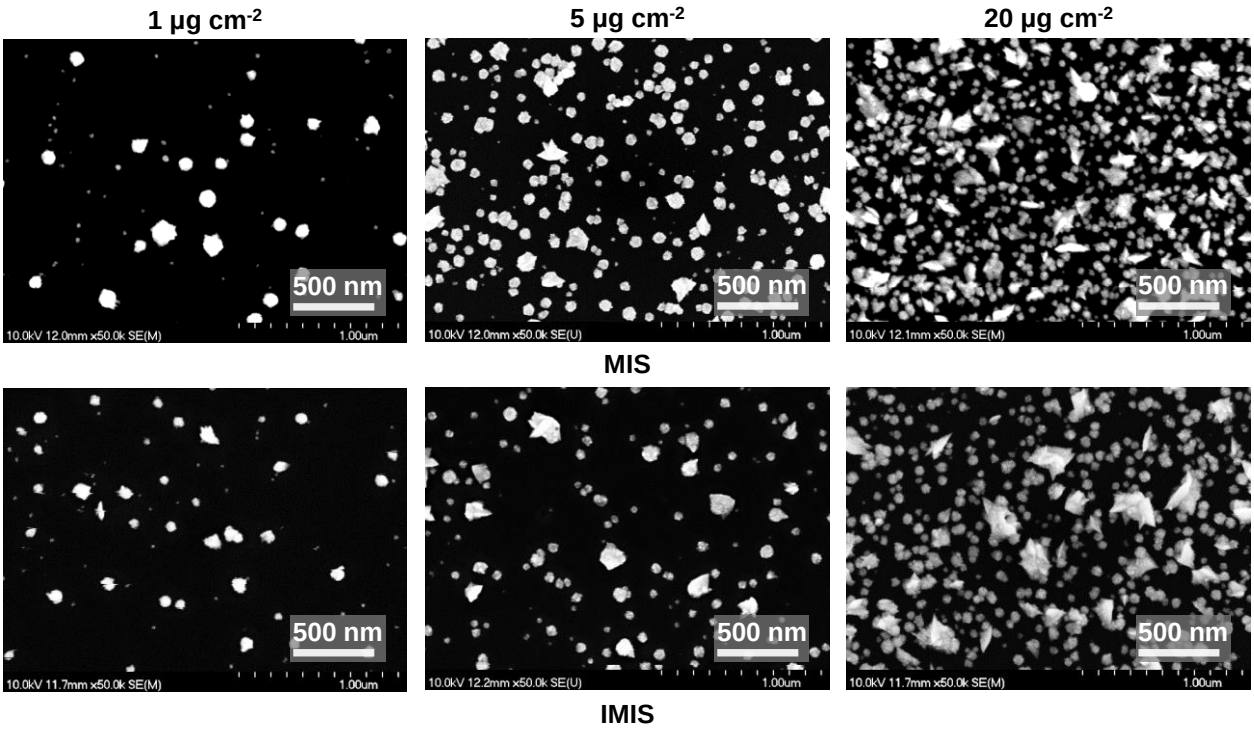

Figure S2. Top view SEM images. Representative SEM images of MIS photoelectrodes with Pt loadings of 1, 5, and 20 μg cm^{-2}.

Table S1. Summary of Pt structure characterization from SEM image analysis based on SEM images taken at a magnification of x50.0k times.

	SiO_x thickness (nm)	Particle coverage (%)	Particle density (particle μm^{-2})	Average Pt nanoparticle diameter (nm)	Average distance between particles (nm)	Surface area (cm^2 Pt/ geometric area cm^2)	Pt loading (μg cm^{-2})
MIS	0	3.3 ± 0.8	17 ± 3	38 ± 32	180 ± 20	0.14 ± 0.03	1.0 ± 0.3
MIS	0	15 ± 3.1	42 ± 8	55 ± 36	86 ± 16	0.63 ± 0.14	5.1 ± 1.4
MIS	0	42 ± 1.2	74 ± 3	66 ± 54	30 ± 1	1.82 ± 0.05	22 ± 0.8
IMIS	2	3.9 ± 0.6	22 ± 2	37 ± 30	155 ± 13	0.17 ± 0.02	1.1 ± 0.2
IMIS	2	13 ± 0.9	35 ± 3	58 ± 34	95 ± 6	0.54 ± 0.04	3.9 ± 0.2
IMIS	2	32 ± 1.6	52 ± 7	70 ± 53	49 ± 4	1.36 ± 0.07	18 ± 3.6
IMIS	5	13 ± 0.2	28 ± 3	65 ± 42	102 ± 4	0.58 ± 0.01	5.0 ± 0.2
IMIS	10	14 ± 1.1	41 ± 5	53 ± 38	86 ± 7	0.59 ± 0.05	4.4 ± 0.5

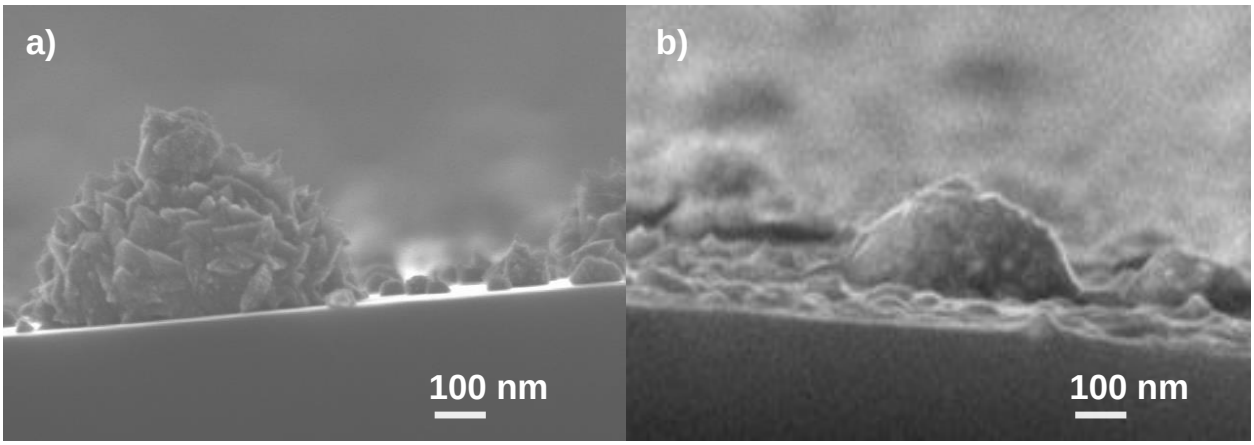

Figure S3. MIS and IMIS side-view. Representative cross sectional FE-SEM images of a) MIS and b) IMIS samples generally reveal smoother Pt nanoparticle features on the IMIS surface than compared to the MIS surface. The smooth features indicate the SiO_2 overlayer coating over and around most of the spikey Pt nanoparticles as suggested by the schematics in Figure 1a and b.

2.2 Characterization of SiO_x thin films by XPS

X-ray photoelectron spectroscopy (XPS) measurements were conducted with a Kratos AXIS Ultra DLD XPS system that was operated at a base pressure of 3×10^{-10} Torr using a monochromated $Al_{K\alpha}$ source (X-ray power 13 kV, 8 mA) and without a neutralizer (Fig. S4). The pass energy was 10 eV and the drain current through the sample stage was 0.4 nA. The XPSpeak program was used in evaluating the peak areas of Si 2p, C 1s, O 1s, and Pt 4f spectra based on Shirley's algorithm for background subtraction. The peak shifts to higher binding energies corresponds to sample charging without the neutralizer, however this did not compromise the atomic ratio analysis (Table S2). The peak area ratios were calculated after accounting for the atomic sensitivity factors (ASF_i) (ASF_{Si} = 0.301, ASF_C = 0.296, ASF_O = 0.891, ASF_{Pt} = 5.575). The Si and O atomic sensitivity factors were obtained using a HF etched Si standard and a wet thermal oxide film (≈300 nm SiO_2 on Si and Ar sputtered at 500 eV for 3 min), whose stoichiometry was assumed to be exactly SiO_2. XPS was used to interrogate the composition of the additional SiO_x layer. The PDMS was converted into SiO_2 with trace amounts of carbon remaining. The $SiO_x/SiO_2/Si$ (IIS) contained 50% higher C 1s signal compared to samples

containing native SiO_2 (IS) where the carbon only arises from adventitious carbon compounds. Additionally, the Pt 4f signal was suppressed by 50% for the $SiO_x/Pt/SiO_2/Si$ (IMIS) compared to the $Pt/SiO_2/Si$ (MIS) sample indicating some SiO_x overlayer coverage on top of the Pt particles.

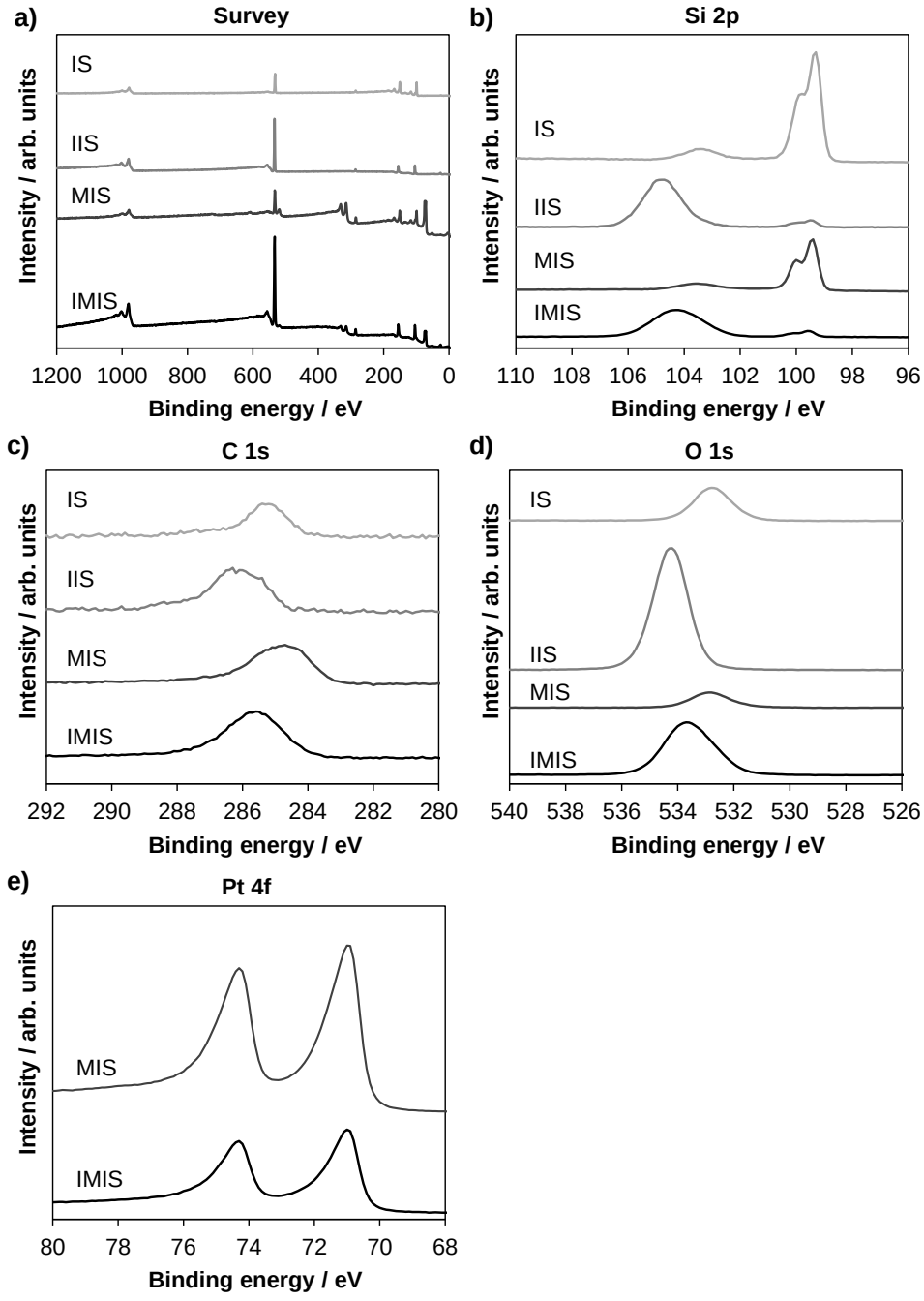

Figure S4. XPS results. X-ray photoelectron spectra of 10 nm SiO_x/native SiO_2/p-Si(100) a) Survey, b) Si 2p, c) C 1s, d) O 1s, and e) Pt 4f. Red curves: $SiO_x/SiO_2/Si$, Black curves: native SiO_2/Si, Grey curves: CASA fitted peaks.

Table S2. Surface composition of samples with and without the SiO_x overlayer determined by XPS measurements. The SiO_x thickness of IIS and IMIS samples is 10 nm. The Pt loading for MIS and IMIS samples is 5 μg cm^{-2}. All compositions are expressed as atomic percentages as described in the text

sample		% metallic Si	% Si in SiO_2	% C	% O	% Pt	O:(Si in SiO_2) ratio
IS	SiO_2/Si	48	7	9	36	0	5.0
IIS	$SiO_x/SiO_2/Si$	2	25	7	66	0	2.6
MIS	$Pt/SiO_2/Si$	33	9	22	27	9	3.0
IMIS	$SiO_x/Pt/SiO_2/Si$	2	26	15	55	2	2.1

2.3 Scanning transmission electron microscopy (STEM)

The cross section STEM sample (typically 50 nm in thickness) was prepared by focus ion beam (FIB) FEI Nova 600 NanoLab. An extra Pt-C protection layer was deposited by FIB to protect the sample surface; this overlayer directly contacted the Pt particles in some areas and was separated by a carbon film in other areas to clearly show the chemical compositions on the sample surface. High-angle annular dark-field (HAADF)-STEM images were acquired from the prepared lamellas using a probe corrected FEI Titan 80−300 microscope operated at 300 kV with spatial resolution of 0.1 nm. The probe convergence angle was 24 mrad and the HAADF detector collected signals between 70 mrad and 400 mrad. Energy Dispersive X-ray Spectroscopy (XEDS) spectral images were collected by Octane T Optima from EDAX, which provides a windowless detector with solid angles up to 0.5 sr. After background subtraction, The Pt and Si maps are generated by summing their M (2075 eV) and K (1740 eV) peaks respectively (window width 150 eV).

Figure S5a shows the presence of Pt clusters and a SiO_x layer deposited onto of the native SiO_2/p-Si substrate for the 10 nm SiO_x/5 μg cm^{-2} Pt/native SiO_2/p-Si(100) sample. The observed SiO_2+SiO_x thickness varies across the sample. In areas of high Pt particle density (left side), the layer is thicker (up to 17 nm). In areas where Pt particles are relatively far away (right side), the SiO_x thickness is thinner (≈9 nm). This average thickness measured by STEM (11 ± 2nm) is

similar to the value measured using spectroscopic ellipsometry (thickness ≈10 nm) on a sample area with no Pt, a finding that can be attributed to the uniformity of the SiO_x layer in relatively smooth areas. Figure S5b shows the details of a typical IMIS structure. The elemental sensitive contrasts between Pt and Si clearly reveals the presence of a well-defined native SiO_2 layer under Pt clusters with a thickness of ≈1.5 nm and a combined SiO_2+SiO_x overlayer thickness of ≈12 nm. The varied contrast inside the Pt cluster implies that the Pt cluster is porous or consisting of small Pt nanoparticles. This porous structure with large surface area would enhance the catalysis properties of Pt clusters. The Pt area marked by the blue arrow in Figure S5c coincidentally laid in the zone axis to show clear 2D atomic column distribution, while in neighboring areas marked by black arrows the Pt particles are disoriented with different lattice. Additional STEM images (Fig. S5d) show that some larger particles protrude out of the SiO_x shell.

The IMIS structure is also directly revealed by STEM-XEDS mapping (Fig. S6). Figure S6a clearly shows the Pt cluster is hemispherical on top of the native SiO_2 layer. The Si map illustrates a weak shell structure on top surface of the Pt, where the Si signal distributes on the surface of Pt cluster (Fig. S6b). Si signal is strongly observed on the Pt contacting corners to the SiO_2 layer (marked by white arrows in Figure S6c. The XEDS spectra shown in Figure 6d are from representative Site I (on Pt cluster), Site II (on the Si shell), and Site III (on the SiO_2 layer) from Figure 6c. This XEDS spectra clearly shows that the Si-K peak signal is weak at the center of the Pt cluster and is relatively stronger on its outer shell. This evidence confirms that the Pt cluster is buried inside a thin SiO_x layer as illustrated in Figure 1d.

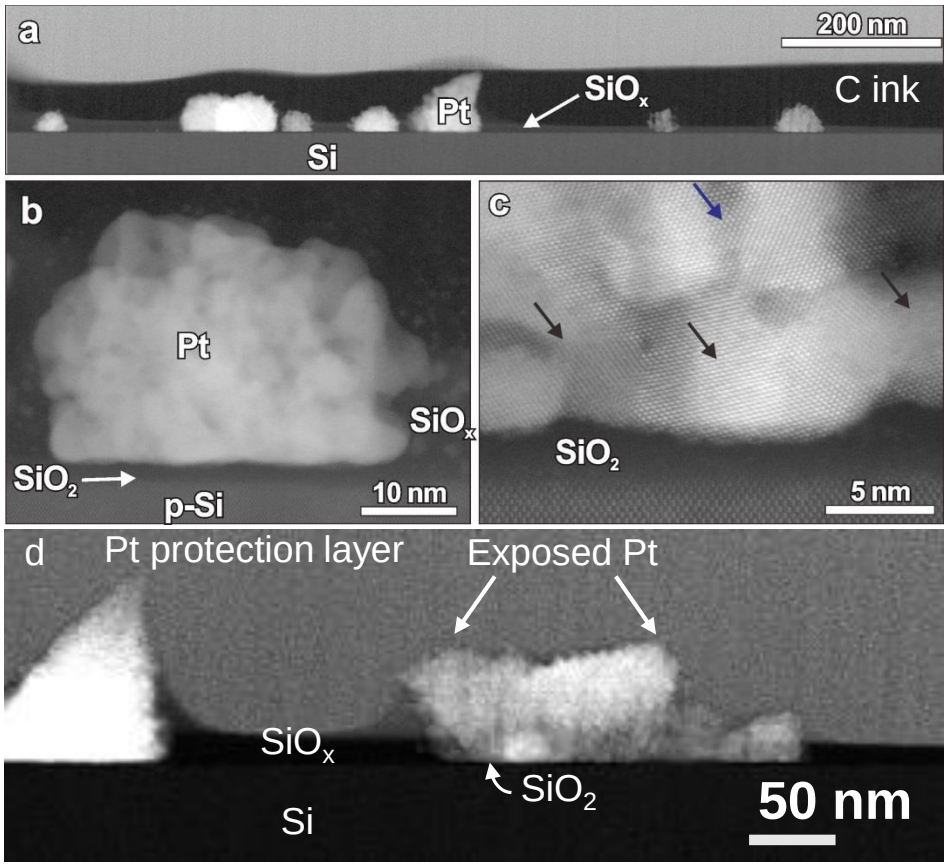

Figure S5. Cross section of the IMIS photoelectrodes revealed by HAADF-STEM. a) Low magnification STEM images of a 10 nm SiO_x/Pt/native SiO_2/p-Si IMIS sample showing the SiO_x overlayer on native SiO_2/Si substrate. b) High resolution HAADF-STEM showing the structure details of an IMIS photoelectrode. c) Atomic resolved HAADF-STEM illustrates that the Pt cluster consists of small Pt particles oriented differently. d) Additional STEM image revealing some larger particles protrude out of the SiO_x shell.

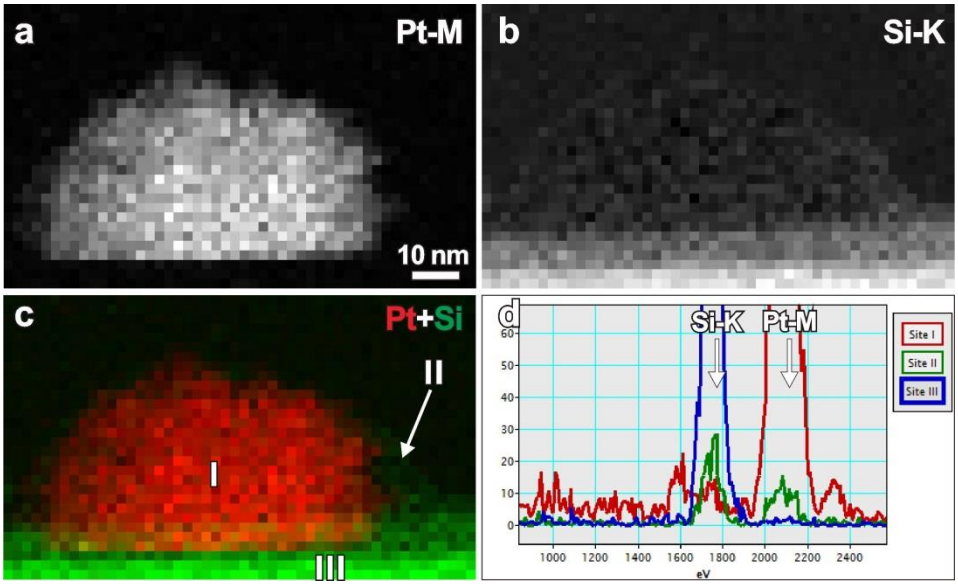

Figure S6. STEM-XEDS mapping of an IMIS photoelectrode. a) The Pt map showing a cluster of Pt on top of SiO_2 layer. b) The Si map shows a weak shell structure on the top surface of Pt cluster. c) The overlay of Pt (red) and Si (green) maps show the relative distribution of those two elements. d) The XEDS spectra from 3 representative sites showing the different presence of Si and Pt signal.

III. Photoelectrochemical characterization

3.1 Photoelectrochemical test procedures

The light was calibrated to AM 1.5G illumination intensity using a VLSI Si reference cell (VLSI Standards, SRC-1000-RTD-QZ) and a Newport AM 1.5 filter (Newport, 81094). Electrodes were tested in deaerated 0.5 mol L^{-1} sulfuric acid (H_2SO_4, Fisher Scientific, ACS grade), prepared from 18 MΩ deionized water (Millipore, Milli-Q Direct 8). The solution was bubbled with nitrogen gas for 20 minutes to purge dissolved oxygen. During measurements the head space of the working electrode compartment was continuously purged with N_2. A Pt mesh counter electrode was located in a secondary compartment separated by a glass frit to prevent product crossover. An Ag|AgCl reference electrode was located in the main compartment. For the 12 hr chronopotentiometry (CP) stability test a reversible hydrogen electrode (RHE) was used as a reference electrode instead of Ag|AgCl to minimize possible Ag contamination during the extended testing period. The

electrolyte was stirred with a magnetic stir bar during PEC testing. The following measurements were performed on each sample: CV (5 cycles between +0.40 V and -0.05 V versus Ag/AgCl at 50 mV s^{-1}), three LSVs under illumination and one in dark (+0.30 to -1.23 V versus Ag/AgCl at 20 mV s^{-1}), and a CV (1 cycle, +0.40 V to -1.23 V vs. Ag/AgCl at 20 mV s^{-1}). In addition, a stability test was conducted by operating the photoelectrodes at a constant current of -10 mA cm^{-2} for 1 hour under illumination. During the test, the open circuit potential was sampled twice for one minute periods. An LSV was performed under illumination before and after the stability test. All LSVs presented in the manuscript and SI are iR corrected, unless otherwise noted.

3.2 PEC performance of control samples

A 5 μg cm^{-2} Pt/native SiO_2/p-Si(100) MIS sample was treated with identical processing steps as the IMIS samples with SiO_x, except that no PDMS was spin coated onto the MIS sample. Toluene was spin coated onto the MIS sample, dried in a vacuum oven at 70 °C for 60 minutes, and treated with UV-ozone for 2 hrs. This UV-ozone treated MIS sample and 'x' nm SiO_x/native SiO_2/p-Si control samples without Pt were evaluated with LSVs in 0.5 mol L^{-1} H_2SO_4 under 1 sun of AM 1.5G illumination (Fig. S7). Poor performance confirms the difference in performance between IMIS and MIS samples was due to the presence of the SiO_x overlayer on Pt particles and not a result of the UV-ozone treatment nor HER catalysis associated with residual carbonaceous species in the SiO_x.

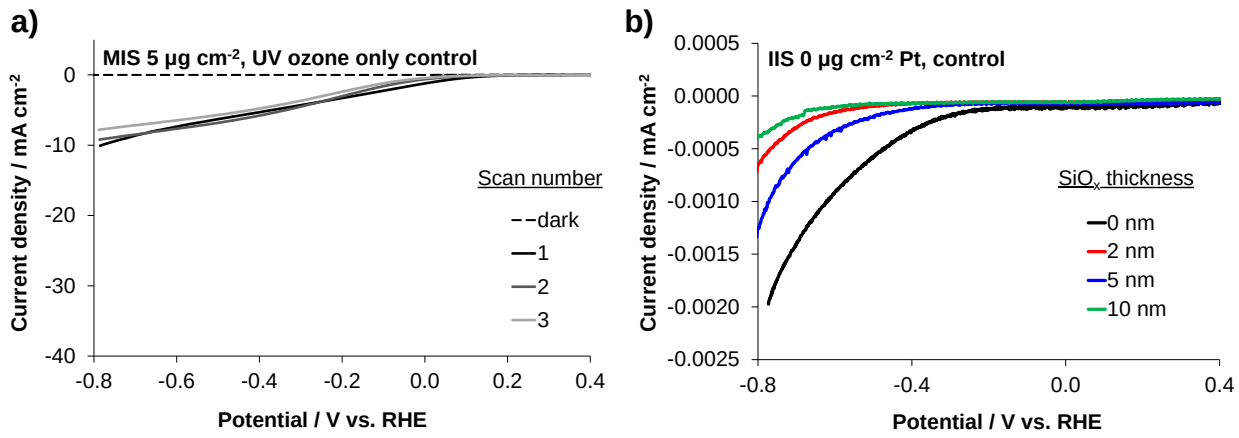

Figure S7. PEC performance of UV-ozone treated MIS and bare SiO_2 control samples. LSV measurements in 0.5 mol L^{-1} H_2SO_4 under 1 sun of AM 1.5G illumination for a) UV-ozone treated MIS 5 µg cm^{-2} Pt/native SiO_2/p-Si(100) and b) 'x' nm SiO_x/native SiO_2/p-Si(100) control samples.

3.3 Stability comparison of MIS and IMIS photoelectrodes

To characterize the stability of each electrode, three consecutive LSVs were conducted and compared (Fig. S8). To quantify photoelectrode stability, the operating potentials at -10 mA cm^{-2} for the first and third LSV were compared. All of the IMIS photoelectrodes demonstrated remarkable stability. This is a significant improvement in comparison to the stability of the MIS photoelectrodes, which depended heavily on the Pt loading. Interestingly, the 20 µg cm^{-2} Pt loaded MIS photoelectrode, with 42 % coverage, was reasonably stable, possibly due to an increase surface area contact/junction area between the Pt nanoparticles and the SiO_2/p-Si substrate. In contrast, the 1 µg cm^{-2} Pt loaded MIS photoelectrode, with only 3 % Pt coverage, was very unstable.

Figure S9 shows the measured potential required for the MIS and IMIS photocathodes to produce -10 mA cm^{-2} in 0.5 mol L^{-1} H_2SO_4 under 1 sun of AM 1.5G illumination. The samples were subjected to open circuit intermittently to simulate the periodic cycling conditions of day and night. The MIS samples without the SiO_x overlayer failed to maintain a constant potential, whereas the IMIS samples with the SiO_x overlayer were able to sustain a consistent potential for 1 hr, the

duration of these stability tests. The 5 μg cm^{-2} Pt loaded MIS sample exhibited sudden potential fluctuations due to the build-up and release of large hydrogen bubbles from the photoelectrode surface. All of the IMIS samples effectively removed hydrogen gas bubbles away from surface due to the hydrophilic nature of the SiO_x over layer, as supported by the nominal potential fluctuations. The lowest Pt loaded MIS sample demonstrated an unexpected behavior where the operating potential decreased after the pulse to OCP.

Although neither the MIS nor IMIS samples dramatically failed during the chronopotentiometric (CP) stability tests, LSVs performed before and after the CP measurements revealed a substantial decrease in performance for the MIS samples but not for the IMIS samples (Fig. S10). The observation of more severe performance degradation under potential cycling (i.e. LSV curves) compared to a long constant current measurement is consistent with those observed in Fig S8. This degradation with LSVs is observed with all the MIS samples shown by the negative 260 mV shift at -10 mA cm^{-2} for the 5 μg cm^{-2} Pt loaded MIS sample (Table 1). In contrast, the IMIS sample with the 10 nm SiO_x overlayer demonstrated the lowest degradation with only a 5 mV shift at -10 mA cm^{-2}.

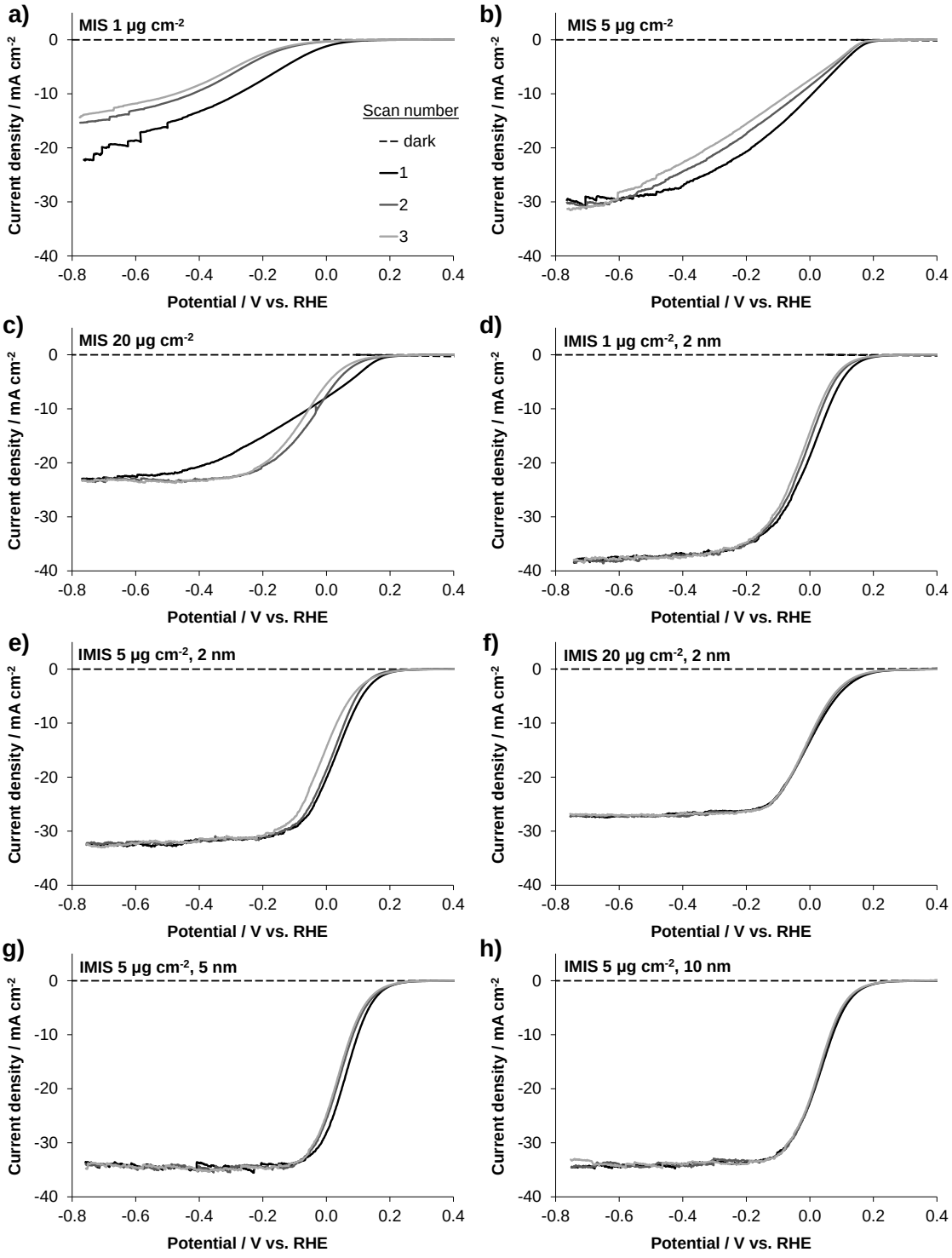

Figure S8. MIS and IMIS performance. LSV measurements in 0.5 mol L^{-1} H_2SO_4 under 1 sun of AM 1.5 G illumination for 'x' nm SiO_x/'y' µg cm^{-2} Pt/native SiO_2/p-Si(100) for various amounts of Pt loading from 1 to 20 µg cm^{-2} and various SiO_x thicknesses from 0 nm to 10 nm. Dark LSVs and LSV's 1, 2, and 3 are shown. a-c) 1, 5, and 20 µg cm^{-2} Pt with 0 nm SiO_x, d-f) with 2 nm SiO_x, and g-h) 5 µg cm^{-2} Pt with 5 and 10 nm SiO_x. The LSV scan rate was 20 mV s^{-1}.

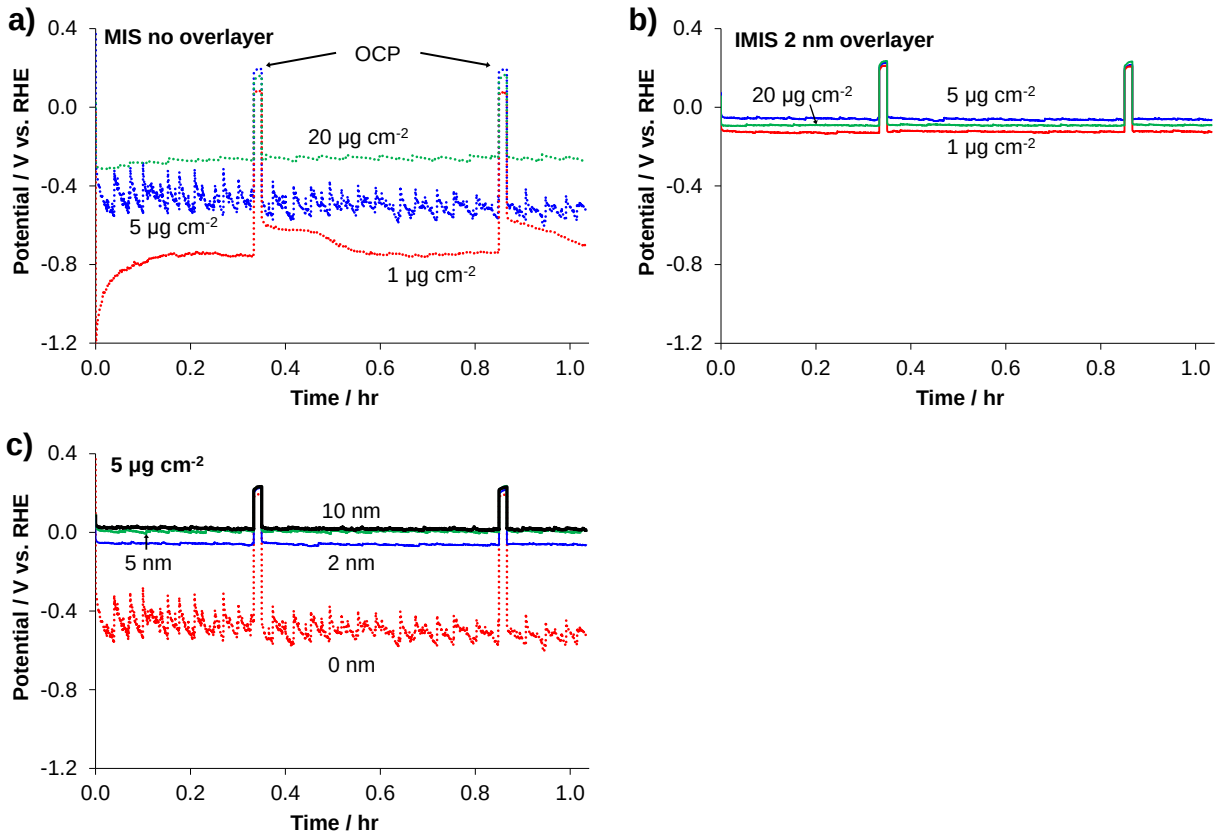

Figure S9. Stability tests. Chronopotentiometery (CP) stability measurements in 0.5 mol L^{-1} H_2SO_4 for a) MIS Pt/native SiO_2/p-Si(100) and b) IMIS 2 nm SiO_x/ Pt/native SiO_2/p-Si(100) for various amounts of Pt loading, and for c) 'x' nm SiO_x/5 μg cm^{-2} Pt/native SiO_2/p-Si(100) for various SiO_x thicknesses from 0 to 10 nm operating at -10 mA cm^{-2} for 1 hr under 1 sun of AM 1.5G illumination. Open-circuit potentials were measured twice for 1 minute during the study. The larger fluctuations in potential for the MIS photoelectrode are caused by differences in bubble growth and detachment.

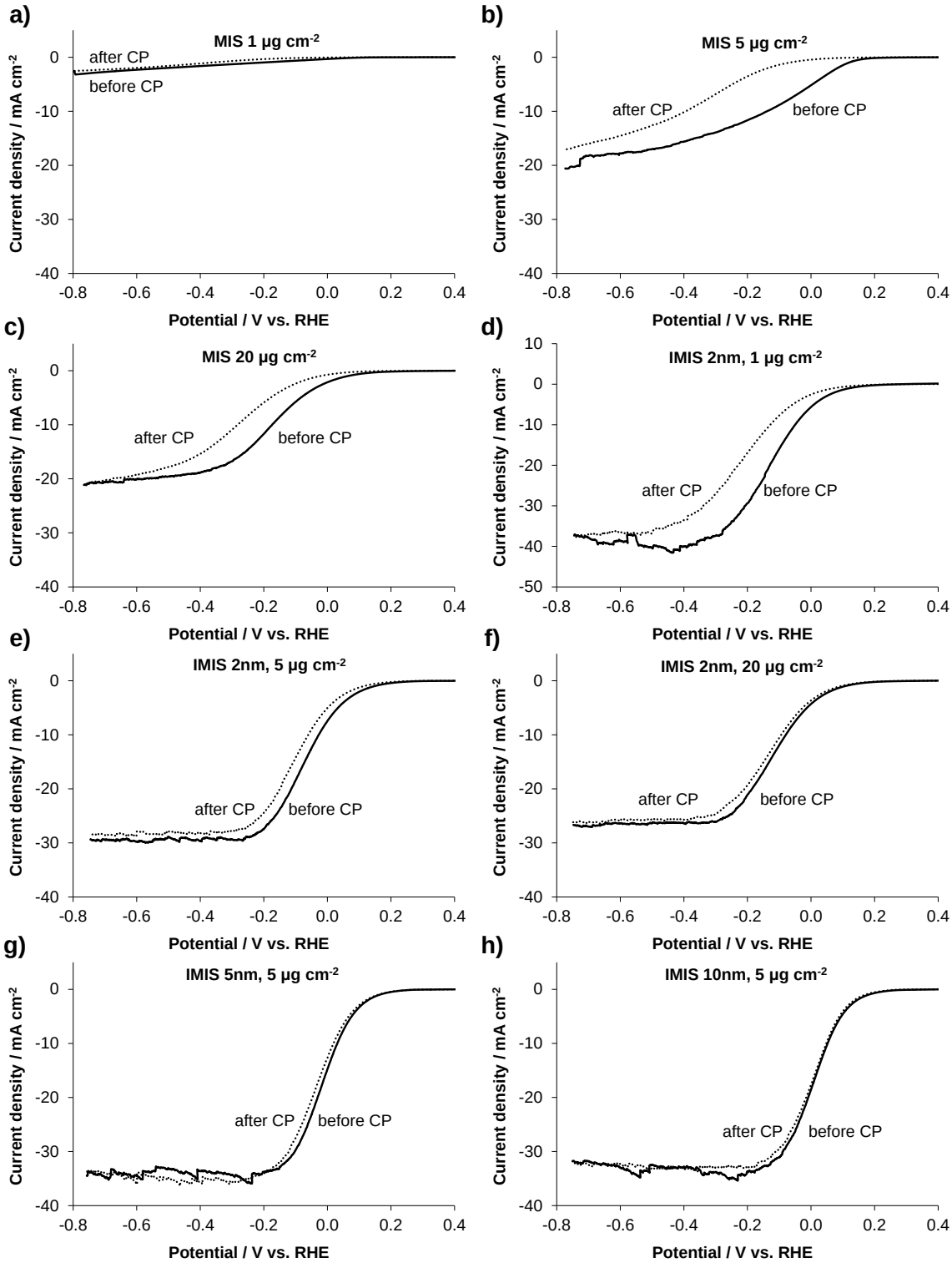

Figure S10. LSV before and after stability test. LSV measurements in 0.5 mol L^{-1} H_2SO_4 under 1 sun of AM 1.5G illumination for 'x' nm SiO_x/'y' µg cm^{-2} Pt/native SiO_2/p-Si(100) for various amounts of Pt loading from 1 to 20 µg cm^{-2} and various SiO_x thicknesses from 0 to 10 nm. a-c) 1, 5, and 20 µg cm^{-2} Pt with 0 nm SiO_x, d-f) with 2 nm SiO_x, and g-h) 5 µg cm^{-2} Pt with 5 and 10 nm SiO_x. The LSV scan rate was 20 mV s^{-1}.

Table S3. Summary of Pt structure characterization from SEM image analysis for samples in Fig. 3b

	SiO_x thickness (nm)	Particle coverage (%)	Particle density (particle μm^{-2})	Average Pt nanoparticle diameter (nm)	Average distance between particles (nm)	Surface area (cm^2 Pt/ geometric area cm^2)	Pt loading ($\mu g\ cm^{-2}$)
MIS	0	31 ± 1.4	71 ± 7	61 ± 43	41 ± 3	1.37 ± 0.05	12 ± 0.9
IMIS	10	29 ± 1.1	82 ± 7	47 ± 47	44 ± 2	1.15 ± 0.06	12 ± 1.5

IV. Understanding origins of poor PEC performance by MIS photoelectrodes

4.1 Light absorption and catalysis

In order to understand the optical properties of low-loading electrodeposited Pt nanoparticles, the light transmittance was measured through electrodeposited Pt on transparent indium tin oxide (ITO) with a UV-Vis Spectrophotometer (Agilent Cary 60) (Fig. S11a). Pt was electrodeposited by methods described in section 1.2 and characterized by SEM to confirm similar Pt loadings with the MIS and IMIS samples used in this study. The 5 $\mu g\ cm^{-2}$ Pt/ITO/glass sampled only showed a 10-15 % decrease in transmittance from the ITO/glass control. These values are in accord with the limiting photocurrent densities observed for the 5 $\mu g\ cm^{-2}$ Pt loaded IMIS samples during photoelectrochemical testing, ranging between 34-37 mA cm^{-2}.

The catalytic activity of the 5 $\mu g\ cm^{-2}$ Pt/ITO/glass sample towards the HER was evaluated by conducting LSV measurements in 0.5 mol L^{-1} H_2SO_4 (Fig. S11b). Only a 60-75 mV overpotential was required to achieve high current densities of interest (20-40 mA cm^{-2}), far less than the 440 mV to 200 mV shift (at -20 mA cm^{-2}) in the MIS photoelectrode LSV curves with respect to their IMIS counterparts having the same Pt loading. These measurements on the Pt/ITO control samples show that that neither light absorption nor kinetic overpotential losses can explain the poor performance of the MIS photoelectrodes. In addition to the high catalytic activity, the HER performance was also stable for the three consecutive LSVs. The stable performance observed in these LSV curves proves that the uncoated Pt particles can be stable under the

conditions tested, and that the unstable behavior exhibited by the MIS samples cannot be attributed to poisoning by solution contaminants.

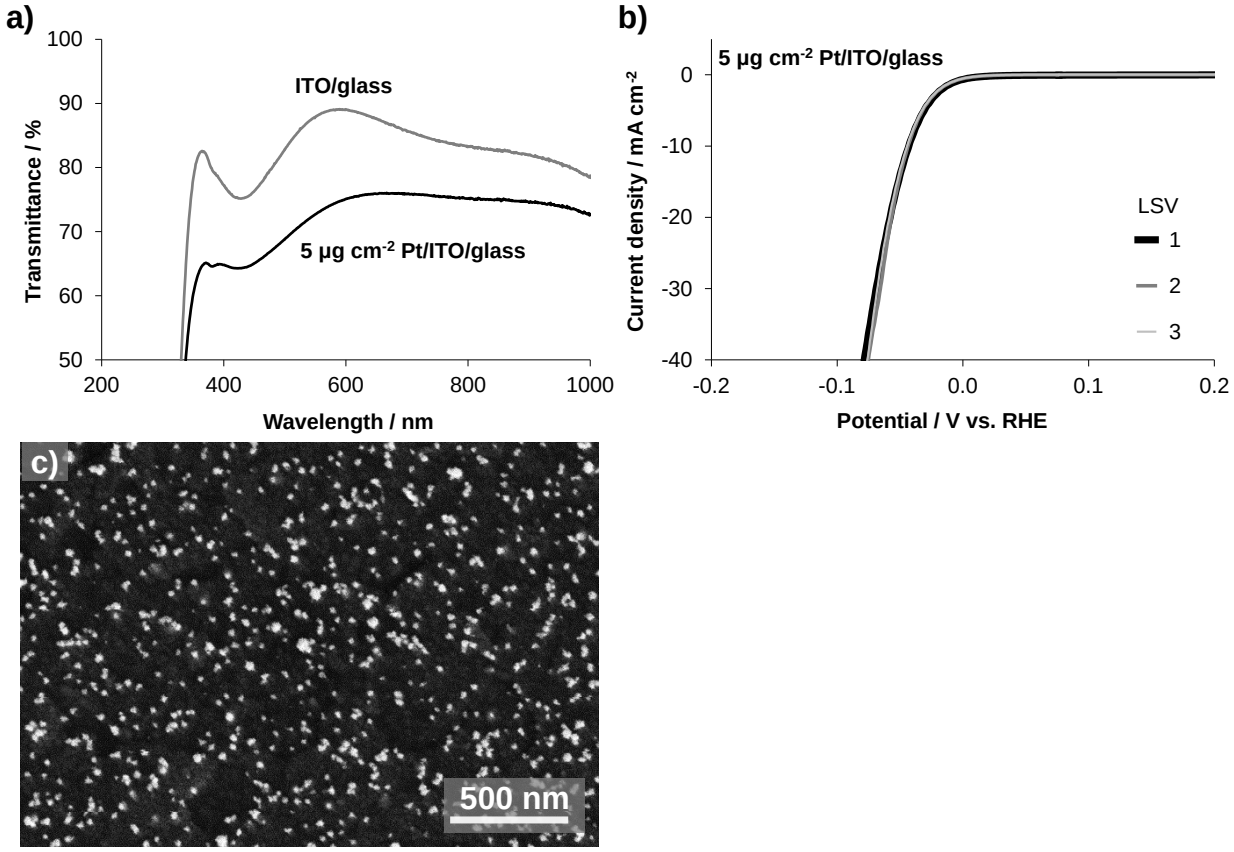

Figure S11. Light transmittance and catalytic activity of electrodeposited Pt particles. a) UV-Vis on Pt/transparent indium tin oxide (ITO) and b) LSV measurements in 0.5 mol L^{-1} H_2SO_4 for 5 µg cm^{-2} Pt/ITO/glass sample. LSV scan rate was 20 mV s^{-1}. c) SEM image of Pt/ITO/glass.

4.2 Effective diffusion length measurements

Effective minority carrier diffusion lengths (L_e) were determined using scanning photocurrent microscopy (SPCM) measurements. In these experiments, an e-beam deposited Pt/Ti front contact was contacted by a tungsten probe, and laser beam-induced photocurrent (J_{ph}), was measured under constant applied voltage (-1 mV) as a function of laser beam distance from the edge of the circular contact (D_L). A schematic of the measurement set-up is provided in Figure

S12a. L_e was calculated from the slope of a plot of the logarithm of normalized photocurrent, $\ln(J_N)$, versus D_L.[5]

L_e is strongly dependent on both the bulk diffusion length of the semiconductor and the surface recombination velocities associated with interfaces in the devices.[5] In this study, the bulk diffusion lengths of the p-Si(100) substrates are expected to be the identical for all samples, but the surface recombination velocity can be very different based on the nature of the SiO_2/p-Si(100) interface. No influence of the SiO_x/native SiO_2/p-Si interfaces is evident in Figure S12b, where a plot of $\ln(J_N)$ versus D_L for a 3 nm Pt/2 nm Ti/native SiO_2/p-Si MIS sample is very similar from that of an IMIS sample containing an additional 10 nm SiO_x overlayer. From the slopes of these $\ln(J_N)$ versus D_L plots, the average values of L_e were 103 μm ± 19 μm for the MIS sample and 103 μm ± 19 μm for the IMIS sample. Effective diffusion lengths were calculated based on slopes between 20 μm < D_L < 50 μm and for MIS and IMIS. Confidence intervals are provided at the 95 % confidence level and are derived from L_e values obtained from three measurements on each sample.

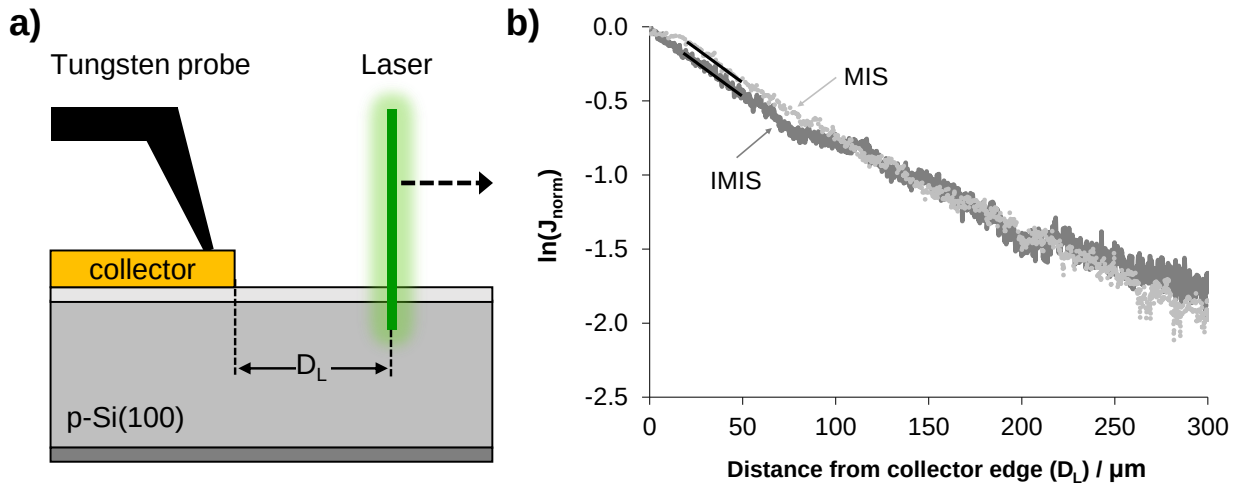

Figure S12. L_e measurements on MIS and 10 nm IMIS. a) Side-view schematic of SPCM measurement set-up used for determining the effective diffusion length in MIS and IMIS control samples in which the metal component, or collector, consisted of e-beam deposited 500 µm bilayer islands with 3 nm Pt on top of 2 nm of Ti. b) Plots of $\ln(J_N)$ versus D_L, measured with a 532 nm laser focused to a beam diameter of ≈3 µm and with incident power of 13.3 µW.

4.3 High electron tunneling current density and voltage penalty

To understand if these MIS photoelectrodes are limited by electron tunneling, the LSVs for MIS samples with different Pt loadings were normalized by the junction areas, as estimated from the SEM-determined particle coverage (Fig. S13). When the current is normalized by the junction area, we refer to this as the "tunneling current density". The samples with 1 and 5 µg Pt cm^{-2}, corresponding to Pt coverages of 3 % and 15 % respectively, demonstrate the highest tunneling current because the junction area is much less than the illuminated area. Moreover, the projected 2D particle area on the SiO_2/p-Si substrate is likely an overestimate of the actual Pt/native SiO_2 junction area (Fig. S5). The small junction areas in the samples with low Pt loadings leads to very high local tunneling current densities, which leads to high overpotentials that are needed to sustain the high current densities.

In order to experimentally view the voltage penalty associated with high tunneling current densities, I-V measurements were conducted in air on a 45 µm diameter 20 nm Pt/30 nm Ti circular

contact that was e-beam deposited onto 2 nm RTO SiO_2/p-Si for varying light intensities. The maximum current density was systematically increased by varying the 532 nm laser illumination intensity. The IV plot of a 20 nm Pt/30 nm Ti/2 nm RTO SiO_2/p-Si sample is shown in Figure S14, where the current density of all samples has been normalized to that of the photo-limited current density. For increasing light intensities, the fill factor decreases significantly, demonstrating that significant voltage penalties are incurred at high tunneling current densities. Although this e-beam deposited Pt/Ti/RTO SiO_2/p-Si sample is not truly representative of the electrodeposited Pt/native SiO_2/p-Si MIS electrodes investigated in this study, the similar MIS architecture and well-defined junction area associated with the circular metal contacts are valuable to directly view the adverse effect that high current densities have on IV curve characteristics.

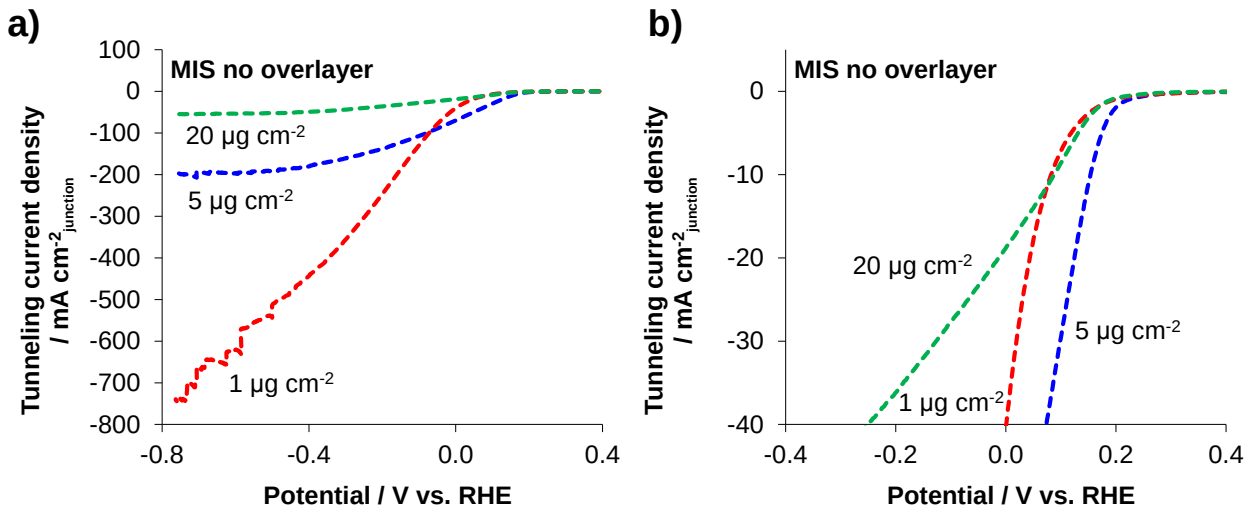

Figure S13. Current densities normalized to net particle area. a) LSV measurements from Fig. 2a for MIS Pt/native SiO_2/p-Si(100) for various amounts of Pt loading normalized by illuminated and junction area and b) a zoomed in plot.

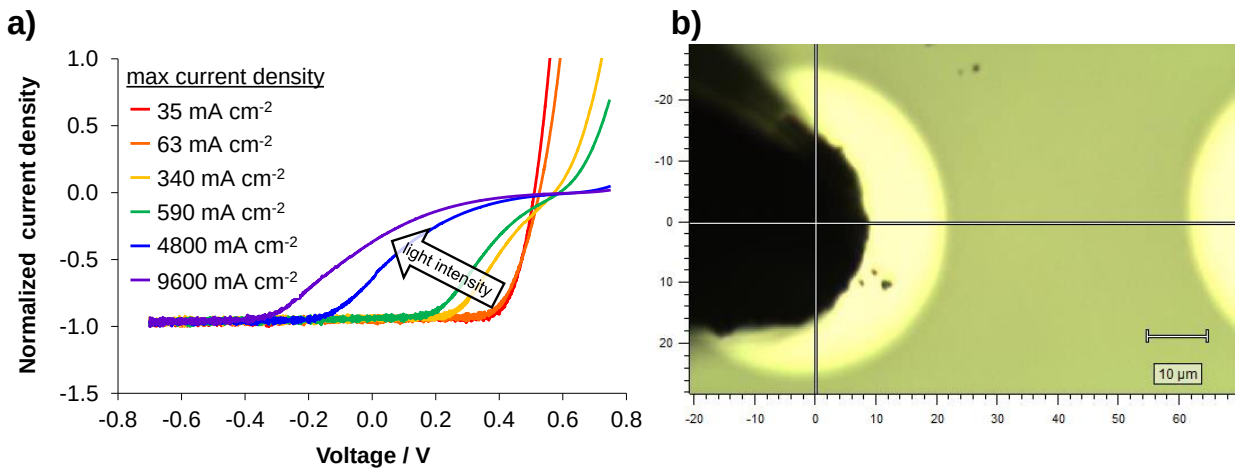

Figure S14. Voltage penalty at large tunneling current densities. a) Normalized I-V measurements in air for a 45 µm diameter 20 nm Pt/30 nm Ti circular contact, that was e-beam deposited onto 2 nm RTO SiO_2/p-Si, under varying intensities of 532 nm laser illumination. The listed current densities are normalized to the junction area, taken to be the area of the e-beam deposited metal contact. b) Optical image of a tungsten probe in contact with a metal contact. I-V curves were measured at a scan rate of 100 mV s^{-1}.

4.3.1 Ferri/ferrocyanide cyclic voltammograms

The total device resistance of physical vapor deposited 3 nm Pt film/2 nm Ti/'x' nm SiO_x/native SiO_2/p-Si electrodes was evaluated by conducting cyclic voltammetry (CV) in a ferri/ferrocyanide solution under AM1.5G illumination (Fig. 4b). Potassium ferricyanide ($K_3Fe(CN)_6$) and potassium ferrocyanide trihydrate ($(K_3Fe(CN)_6 \cdot 3H_2O$ were used to make a 1:1 solution containing 10 mmol L^{-1} of each species with 1 mol L^{-1} potassium chloride. Pt mesh was used as the counter electrode and an Ag|AgCl electrode was used as the reference electrode. All ferri/ferrocyanide CVs were measured at a scan rate of 100 mV s^{-1} in a static solution.

4.3.2 Cyclic voltammetry modelling for device series resistance

The experimental CVs obtained in ferri/ferrocyanide were fit to a standard CV model using EC-lab software V10.40 (Bio-logic). The high-frequency impedance determined series resistance, 11.5 Ω, determined by electrochemical impedance spectroscopy (EIS) for the control sample lacking an SiO_x layer was first used to perform an iR correction on the CV data for all the samples

(note: iR correction was only performed for this analysis; the CV shown in Figure 4 of the main article contain the raw CV data). The CV for the control sample was first fit assuming no additional uncompensated series resistance, a surface area of 0.246 cm^2, reductant and oxidant concentrations of 10 mmol L^{-1}, a scan rate of 100 mV s^{-1}, room temperature, and the charge transfer coefficient $\alpha = 0.50$. The best fit was obtained with $E_0 \approx 0.27$ vs Ag/AgCl/sat. KCl electrode, $k_0 = 0.24$ cm s^{-1},[6] $D_O = 7.1 \times 10^{-6}$ cm^2 s^{-1}, $D_R = 6.1 \times 10^{-6}$ cm^2 s^{-1}. The values of the diffusion coefficients are similar to those reported by Konopka and McDuffie, who studied millimolar concentrations of ferri/ferrocyanide in 1.0 mol L^{-1} KCl on platinum and found $D_O = 7.3 \times 10^{-6}$ cm^2 s^{-1} and $D_R = 6.7 \times 10^{-6}$ cm^2 s^{-1}.[7] The iR-corrected CVs of all SiO_x-containing photocathodes were then fit using the parameters obtained from the fit of the CV for the sample lacking the SiO_x layer, only varying the uncompensated series resistance, taken here to be the "device resistance" reported in Figure 4c. The best fit for the 2 nm, 5 nm, and 10 nm SiO_x-containing samples was achieved with device resistance values of 215 Ω, 225 Ω and 255 Ω, respectively. This fitting procedure is adapted from Scheuermann.[8,9] The simulated CV fit and experimental CV of an electrode containing no SiO_x overlayer material and an electrode with 2 nm SiO_x are shown in Figure S15 a and b respectively.

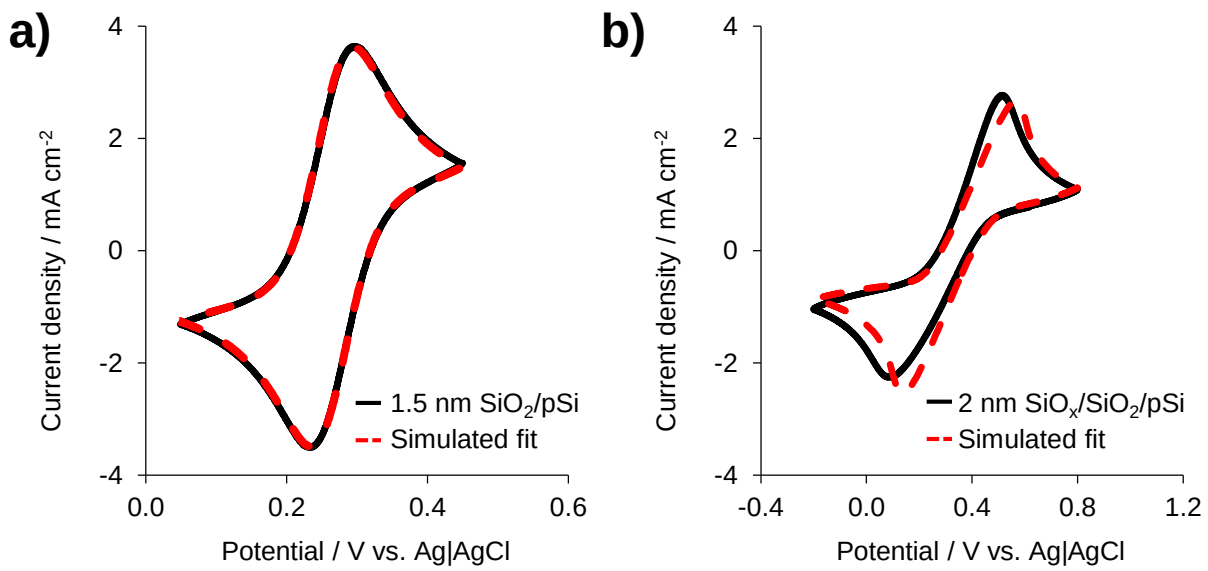

Figure S15. Simulated cyclic voltammograms for total series resistance. CV of a) 3 nm Pt/2 nm Ti/1.5 nm SiO_2/p-Si and b) 3 nm Pt/2 nm Ti/2 nm SiO_x/1.5 nm SiO_2/p-Si in ferri/ferrocyanide solution compared to a simulated fit using EC-lab software. CV scan rate was 100 mV s^{-1}.

V. Understanding degradation in PEC performance of MIS photoelectrodes

5.1 Pt particle adhesion

Figure S16a,b contains SEM images that were taken of identical locations on the surface of an MIS photoelectrode (5 ug Pt cm^{-2}) before and after three consecutive LSV measurements under simulated AM 1.5 illumination (Fig. S16c). Despite the significant degradation in LSV curve properties, no changes in Pt particle location can be observed in Figures S16a,b, indicating that that the Pt nanoparticles visible under the SEM are not agglomerating or detaching from the SiO_2 surface over short time periods. Due to the limited resolution of the SEM, the movement of sub-10 nm Pt particles, which are expected to be most mobile,[10] cannot be ruled out.

However, SEM images of the 12 μg cm^{-2} Pt/native SiO_2/p-Si(100) MIS sample, after 12 hours of operating at -10 mA cm^{-2}, reveal substantial non-uniformities on the surface (Fig. 3c). After the same 12 hour CP test, the 10 nm SiO_x/12 μg cm^{-2} Pt/native SiO_2/p-Si(100) IMIS sample remained very uniform after the 12 hr CP test (Fig. 3d). It should be noted that large (≈200 μm to

2,000 μm diameter) circular non-uniformity features are visible on the degraded MIS sample following the 12 hr CP test. These large circular features are similar to the size of H_2 bubbles that are observed on the photoelectrode surface during operation, suggesting the possibly adverse effect of H_2 bubbles on photoelectrode stability.

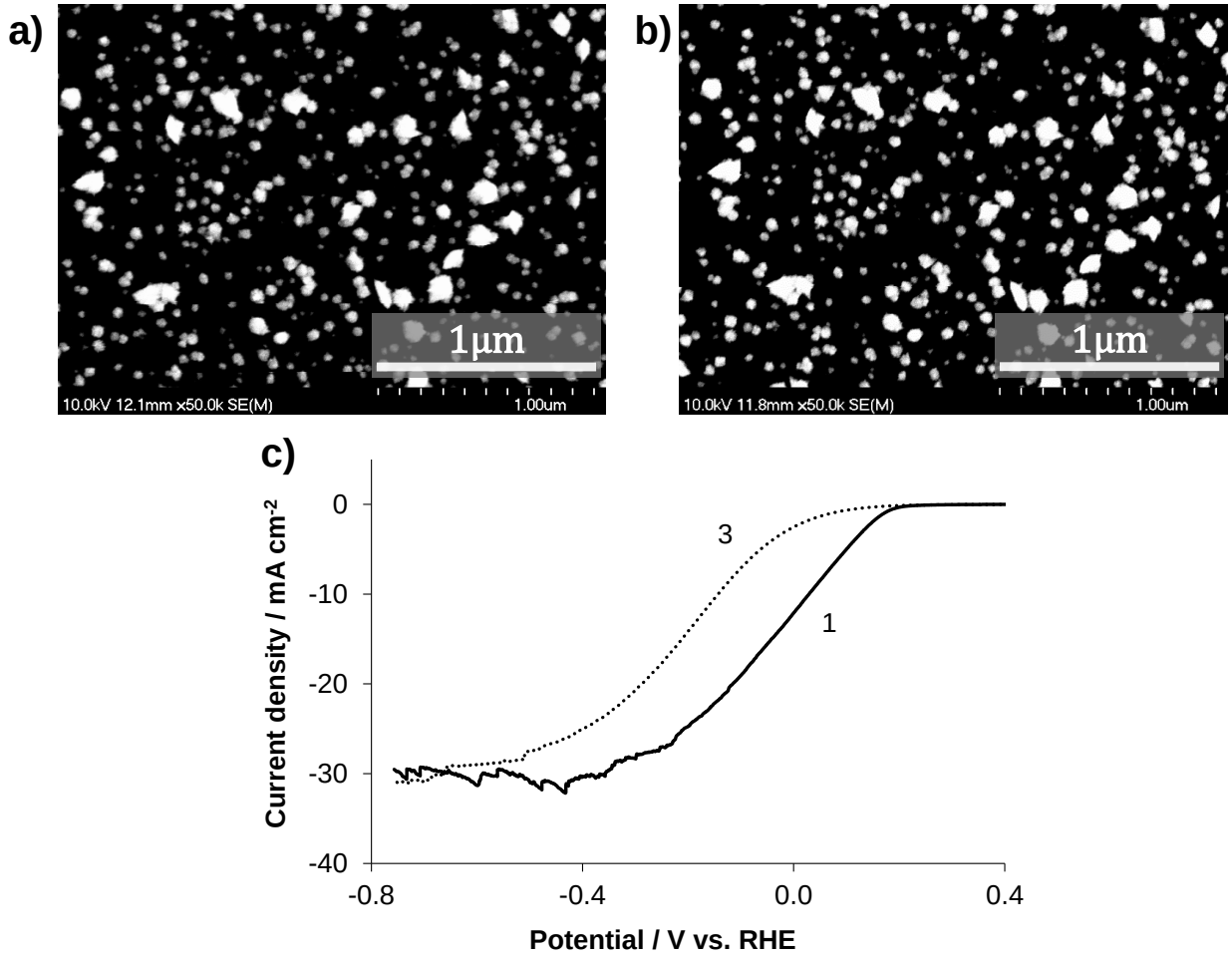

Figure S16. SEM images of MIS photoelectrode before and after PEC LSVs. SEM images of a 5 μg cm^{-2} Pt/native SiO_2/p-Si(100) a) before and b) after 3 LSVs in 0.5 mol L^{-1} H_2SO_4. c) First (solid) and third (dashed) LSV measurements in 0.5 mol L^{-1} H_2SO_4 under 1 sun of AM 1.5G illumination for 5 μg cm^{-2} Pt/native SiO_2/p-Si(100).

5.2 Degradation dependence on operating current density

In order to understand the relationship between MIS degradation and tunneling current density, MIS electrodes with low and high Pt coverages were PEC tested in 0.5 mol L^{-1} H_2SO_4

under 0.25 and 1 sun intensities (Fig. S17). The light intensities were calibrated with a VLSI Si reference cell (VLSI Standards, SRC-1000-RTD-QZ). MIS electrode stability was evaluated by performing five CV cycles between -0.8 V to +0.6 V vs. RHE and monitoring the decrease in operating current density (at a given potential) with each successive cycle. Figure S17a shows minimal degradation for both MIS samples under low light intensity corresponding to low tunneling current density. However, under higher light intensity both samples degrade after 1 CV cycle and is more significant for the lower Pt loading electrode. Table S4 summarizes the Pt loading and coverages (determined by SEM image analysis described in section S1.2) of the samples investigated in this study (Fig. S17). The coverage of the low and high Pt loading samples was ≈12 % and ≈30 % respectively.

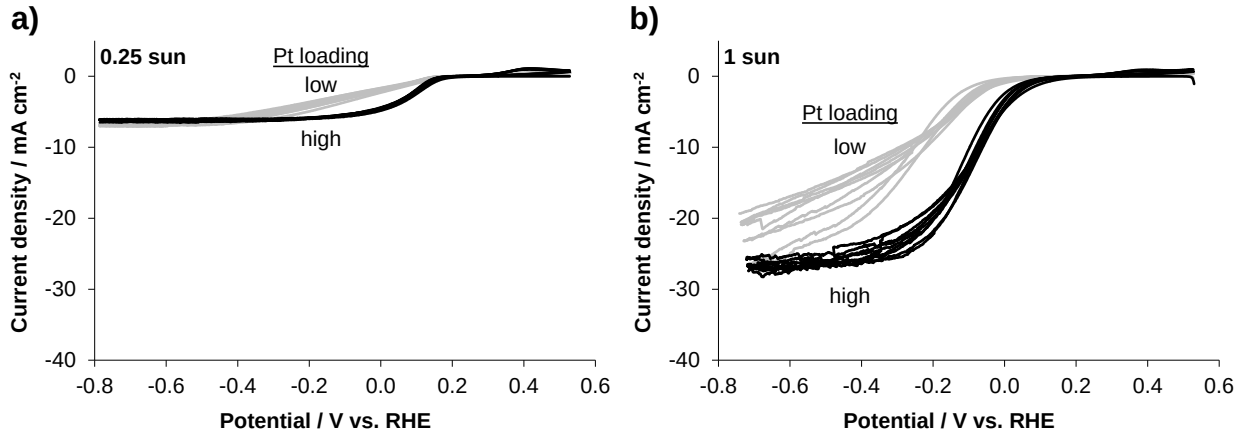

Figure S17. Effect of light intensity on MIS stability. CV measurements in 0.5 mol L^{-1} H_2SO_4 for low and high Pt loaded MIS samples under a) 0.25 sun and b) 1 sun intensity. CV scan rate was 20 mV s^{-1} for 5 cycles. Grey curves: low Pt loading. Black curves: high Pt loading.

Table S4. Summary of Pt structure characterization from SEM image analysis for samples in Fig. S17

MIS Pt loading	Light intensity test (sun)	Particle coverage (%)	Particle density (particle μm^{-2})	Average Pt nanoparticle diameter (nm)	Average distance between particles (nm)	Surface area (cm^2 Pt/ geometric area cm^2)	Pt loading ($\mu g\ cm^{-2}$)
Low	0.25	10 ± 1.1	77 ± 17	27 ± 23	79 ± 10	0.32 ± 0.06	2.1 ± 0.4
Low	1	13 ± 0.6	102 ± 6	25 ± 26	60 ± 3	0.46 ± 0.06	3.4 ± 0.7
High	0.25	29 ± 1.4	74 ± 3	38 ± 39	42 ± 1	1.05 ± 0.06	14 ± 2
High	1	31 ± 1.5	22 ± 2	45 ± 39	40 ± 1	1.19 ± 0.07	13 ± 0.7

References

(1) Mirley, C.; Koberstein, J. *Langmuir* **1995**, *11* (4), 0–3.
(2) Phely-Bobin, T. S.; Muisener, R. J.; Koberstein, J. T.; Papadimitrakopoulos, F. *Synth. Met.* **2001**, *116* (1-3), 439–443.
(3) Ouyang, M.; Yuan, C.; Muisener, R. J.; Boulares, a.; Koberstein, J. T. *Chem. Mater.* **2000**, *12* (29), 1591–1596.
(4) Ustarroz, J.; Altantzis, T.; Hammons, J. A.; Hubin, A.; Bals, S.; Terryn, H. *Chem. Mater.* **2014**, *26* (7), 2396–2406.
(5) Schroder, D. K. *Semiconductor Material and Device Characterization: Third Edition*; 2005.
(6) Daum, P. H.; Enke, C. G. *Anal. Chem.* **1969**, *41* (4), 653–656.
(7) Konopka, S. J.; McDuffie, B. *Anal. Chem.* **1970**, *42* (14), 1741–1746.
(8) Scheuermann, A. G.; Prange, J. D.; Gunji, M.; Chidsey, C. E. D.; McIntyre, P. C. *Energy Environ. Sci.* **2013**, *4* (8), 1166–1169.
(9) Scheuermann, A.; Kemp, K.; Tang, K.; Lu, D.; Satterthwaite, P.; Ito, T.; Chidsey, C. E. D.; Mc Intyre, P. *Energy Environ. Sci.* **2015**.
(10) Ustarroz, J.; Hammons, J. A.; Altantzis, T.; Hubin, A.; Bals, S.; Terryn, H. *J. Am. Chem. Soc.* **2013**, *135* (31), 11550–11561.